ACS Catalysis

Research Article

pubs.acs.org/acscatalysis

Effect of Support Particle Size in Steam Reforming of Ethanol over Co/CeO_2 Catalysts

I. Ilgaz Soykal, Hyuntae Sohn, and Umit S. Ozkan*

Department of Chemical and Biomolecular Engineering, The Ohio State University, 140 W. 19th Avenue, Columbus, Ohio 43210, United States

Supporting Information

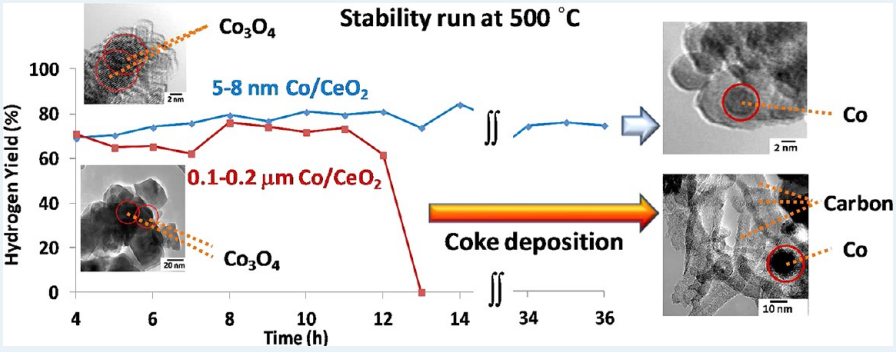

ABSTRACT: Co catalysts supported on ceria supports with two different particle sizes, one in the micro- and the other in the nano-range, were investigated for their ethanol and ethylene steam reforming performance. Pre- and post-reaction characterization techniques, including high-resolution transmission electron microscopy, temperature-programmed oxidation, dispersion, pore size measurements, in situ X-ray diffraction (XRD) and X-ray absorption fine structure spectroscopy (XAFS) studies were performed to examine the reducibility of the catalysts. Steady-state-activity testing has shown nanoparticles to have a higher reforming activity for ethanol, but also high ethylene yields. In spite of the high ethylene yields, catalysts supported on nanoparticles proved to be highly resistant to coking while the catalysts supported on larger ceria particles suffered from coke formation. Reforming experiments performed with ethylene showed significant differences in activity and stability. Bare supports were also tested for activity and the nanoparticle support was seen to have high dehydration activity. *Operando* DRIFTS experiments performed during ESR showed differences in surface species. Pulse experiments performed to use methanol oxidation as a probe reaction suggested differences in the relative abundance of redox sites and basic sites. The bare ceria supports also exhibited significant activity for ethanol dehydration, but not for C−C cleavage. The superior performance of the catalysts supported on nanoparticles is thought to be due to a combination of factors, including increased reducibility, improved metal dispersion, and a difference in relative abundance of redox sites on the surface. All of these properties and, in turn, the catalytic performance, appear to be affected by the particle size of the support.

KEYWORDS: *cobalt, particle size, ceria, ethylene, ethanol steam reforming*

1. INTRODUCTION

Hydrogen production from ethanol steam reforming (ESR) has been studied extensively in recent years.[1−5] Behind this increased interest in using ethanol as a hydrogen source is the potential for deriving it from plant matter. Fuels that can be obtained from biological sources have the advantage of offering a theoretically closed carbon loop since the CO_2 produced during reforming would be sequestered via photosynthesis during plant growth.[6] Different catalytic systems have been investigated for ESR, including both precious metals and non-noble metals. As expected, noble metal catalysts, such as Rh, Pt, Pd, Ru, and Re afford high activities over wide temperature ranges of 400−600 °C with relatively high space velocities.[7−13] However, the fluctuating prices and high costs associated with such metals render non-noble metal-based catalysts, such as Ni, Cu, and Co, as attractive alternatives.[14−21] Among the different transition metals studied, cobalt-based catalysts were found to have high C−C bond cleavage activity in the ESR temperature range of 300−500 °C.[22−28] Previous work in our laboratories focused on the role of synthesis parameters,[29−31] support effects,[32,33] as well as the reaction networks and mechanisms.[34,35] The role of the cobalt coordination environment and reducibility were also examined through in situ techniques.[36] More recent work has focused on determining the effect of support morphology on catalytic ESR activity. In this study, we examine the role of the support particle size and

Special Issue: Operando and In Situ Studies of Catalysis

Received: June 28, 2012
Revised: September 21, 2012
Published: October 2, 2012

   dx.doi.org/10.1021/cs3004159 | ACS Catal. 2012, 2, 2335−2348

reducibility on the catalytic performance as well as the reaction networks involved in ethanol steam reforming.

Particle size effects have been the subject of many studies. Haga et al. have investigated the effect of particle size on the catalytic properties of Co/Al_2O_3, where metallic particle size was controlled by changing the cobalt deposition method and found the selectivity for steam reforming to increase with metallic dispersion.[26] A further study by the same group has shown the crystallite size of cobalt to vary the adsorption strength of ethanol on the sample.[27] Zhou et al. investigated the effect of decreasing CeO_2 particle size between 4 and 60 nm particles and reported increasing oxygen vacancies in the ceria lattice with decreasing particle size, which increased the oxygen mobility on the surface.[37] Flytzani-Stephanopoulos and co-workers have investigated the effect of support morphologies, which also varied in size from 0.1 to 0.2 μm to 30 nm[38−40] and found the Au dispersion as well as particle size to be influenced by support effects in steam reforming of methanol and water gas shift catalysis.

The extent of catalyst reduction under ethanol steam reforming conditions was found to have a significant effect on catalyst performance.[36,41,42] An equilibrium state was reported between CoO and metallic Co during in situ ESR conditions. Recent work by the Vohs group investigated the support effects of ceria on the cobalt species[43] as well as the effect of oxidized and reduced cobalt species on steam reforming product distribution.[44,45]

In this paper, we present results regarding the effect of ceria and cobalt particle size on CeO_2-supported Co catalysts in ethanol steam reforming. Ceria supports, with two different particles sizes, one in the micrometer range and the other in the nanometer range, were used and compared, with and without cobalt loading. Structural characterization was performed by high-resolution transmission electron microscopy (HR-TEM) and in situ X-ray diffraction (XRD), surface area analysis and metallic dispersion measurements. In addition to steady-state reaction experiments, various in situ and operando techniques were used including X-ray absorption fine structure spectroscopy (XAFS) and diffuse reflectance infrared spectroscopy (DRIFTS) experiments. Steady-state-activity tests and post-reaction studies with TEM and temperature-programmed oxidation shed further light onto the performance and stability of the samples for steam reforming. Pulse experiments using on line mass spectrometry (MS) were performed in an effort to use methanol oxidation as a probe reaction. In addition to experiments with ethanol, reaction experiments with ethylene were also performed. Ethylene is widely regarded as a precursor to coking for steam reforming reactions.[34,46−48] As a product of ethanol dehydration, ethylene is a possible byproduct for ethanol steam reforming. Tanaka et al. reported Ni/8YSZ catalysts which are resistant to coke formation under partial ethylene atmospheres for solid oxide fuel cell conditions.[49] Breen et al. investigated metal catalysts such as Rh, Pd, Ni, and Pt supported over ceria and zirconia and reported catalytic systems which are stable under partial ethylene feed.[17]

2. EXPERIMENTAL SECTION

2.1. Catalyst Preparation. Two ceria supports with different particle sizes were prepared. The support with a particle size in the 0.1−0.2 μm range (denoted as CeO_2−MP) was prepared by calcining Sigma Aldrich 99.999% <5 μm CeO_2 at 450 °C for 3 h in air. The support with a particle size in the 5−8 nm range (CeO_2−NP) was prepared via the hydrothermal method[50] where 1.5 g $Ce(NO_3)_3{\cdot}6H_2O$ (Sigma Aldrich 99.9%) was dissolved in 9.4 mL of water and combined with 25 mL of 11 wt % NaOH. The resulting suspension was stirred for 15 min at room temperature where $Ce(OH)_3$ particles precipitated. The solution was kept at room temperature for 24 h before filtration of the solids. The remaining solids were rinsed with approximately 2 L of deionized and distilled water until a pH value of 7 was reached. Following the neutralization step, the solids were dried in air at 90 °C overnight. The dried $Ce(OH)_3$ precursors were calcined at 450 °C for 3 h under air. Impregnation of 10% (by weight, metallic) cobalt on both MP and NP supports was carried out via the incipient wetness impregnation method with $Co(NO_3)_2$ (Aldrich, 99.999%) dissolved in 200 proof ethanol (Decon Laboratories) and applied onto the support in five consecutive steps by drying the impregnated catalyst at 110 °C overnight in between each step to improve the homogeneity of the resulting catalyst. Following the final impregnation and drying step, the catalyst was calcined at 450 °C for 3 h under air flow.

2.2. Catalyst Characterization. *2.2.1. Surface Area, Pore Volume, and Metal Dispersion.* The Brunauer−Emmett−Teller (BET) surface area and pore volume of the samples were measured by a Micromeritics ASAP 2020 (accelerated surface area and porosimetry) instrument, using nitrogen adsorption/desorption isotherms collected at liquid nitrogen temperature. The desorption branch of the isotherm was used to determine the Barret−Joyner−Halenda (BJH) pore size distributions with pore sizes around 18 Å and 8.5 Å for Co/CeO_2(MP) and Co/CeO_2(NP) catalysts, respectively . Before measurement, the catalyst was degassed for 12 h at 130 °C under a vacuum better than 2 μm Hg.

The dispersion measurements were performed using the N_2O chemisorption technique outlined earlier by Jensen et al.[51] For these measurements, 100 mg of the sample was packed in a 1/4″ OD fixed bed quartz reactor with a quartz frit and placed inside a fast-response furnace (Carbolite, MTF 10/15/130). The sample was reduced in situ at 400 °C using 5% H_2 in He for 2 h, which are the same parameters used for reduction pretreatment prior to reaction experiments. The reactor was then flushed with He at the same temperature and cooled under He flow. N_2O chemisorption was performed by introducing a stream of 3% N_2O/He to the reactor at 40 °C. Species in the m/z=12 to m/z=46 range were monitored via an MKS−Cirrus II online mass spectrometer. The mass spectrometer was calibrated for instrumental sensitivity factors. The contribution of N_2O fragment to the m/z = 28 trace has been subtracted to quantify the N_2 amount desorbing from the sample surface. Throughout the experiment, N_2O and N_2 were the only species detected in the reactor effluent. For quantification of the N_2 formation, known volumes of N_2 were injected to the mass spectrometer under the same flow conditions with a 250-μL-sample loop connected to an automated six-port valve. The number of O atoms consumed is calculated through N_2 evolution, and the number of surface Co sites is calculated after the Fickian diffusion correction, assuming a 1:1 Co:O ratio.

2.2.2. TEM. A Phillips Tecnai F20 instrument equipped with a field emission gun and operated at 200 kV was used for transmission electron microscopy (TEM). All images are collected in the brightfield. Samples were suspended in ethanol and were sonicated for 10 min for high dispersion. The resulting emulsion was deposited immediately after sonication on a 200 mesh copper grid coated with lacey carbon to prevent

agglomeration of the particles. ImageJ processing software is used for analysis of the TEM digital micrographs. Particle histograms are obtained by using the "Measure function" of the ImageJ software by using a minimum of 30 particles. For post-reaction characterization, samples that were kept online for a minimum of 12 h were used without further processing.

2.2.3. In Situ XRD. The in situ XRD patterns during reduction of Co/CeO_2(MP) and (NP) samples were collected on a Bruker D8 Advance X-ray diffractometer with monochromatic Cu Kα radiation (λ = 1.5418 Å) through a tube operated at 40 kV and 50 mA and equipped with an Anton Paar HTK1200 controlled-atmosphere oven. A linear heating rate of 7 °C/min was used, and the temperature was held constant at each temperature step for at least 30 min prior to the collection of the diffraction patterns. Both samples were reduced stepwise under 30 cm^3/min 5% H_2/He starting from room temperature in 50 °C increments up to 500 °C. The sample was then cooled under hydrogen flow to room temperature. After flushing the in situ chamber with an inert, temperature programmed reoxidation of the sample was performed with 5% O_2/He following the same temperature steps.

2.2.4. In Situ XAFS. Catalyst samples oxidized or reduced in situ were investigated in terms of their Co coordination environment using controlled-atmosphere X-ray absorption fine structure (XAFS) technique. The spectra were collected for the Co K-edge (7709 eV) at the bending magnet beamline (5BM-D) of the Dow-Northwestern-DuPont Collaborative Access Team (DND-CAT) of the Advanced Photon Source, Argonne National Laboratories. The measurements were made in transmission mode with the Si(111) monochromator detuned by 30% to eliminate the higher order harmonics in the beam. The sample thickness was chosen to give an absorption edge jump of about 0.3 at the Co K-edge. The 10% Co/CeO_2 catalysts were mixed with SiO_2 at a ratio of 1:4 and finely ground (<150 mesh) to obtain a homogeneous mixture. Approximately 8 mg of the mixture was then pelletized using a 6-mm polished steel die and placed inside a 5 cm-long quartz tube (6.5 mm ID) and supported with quartz wool plugs. The sample was then centered in a 45 × 2 cm controlled-atmosphere XAFS chamber that was fitted with Kapton windows. The XAFS reactor setup allowed continuous flow of the reactants as well as the isolation of the catalyst sample.

For both samples the XAFS cell was heated to 400 °C under helium and the XAFS spectra for the oxidized catalyst was collected. The catalyst was then reduced in situ under 3.6% H_2/He for 1 h after which spectrum collection was started. Phase shifts and backscattering amplitudes used for the analysis of the data were obtained from the experimental reference spectra collected on reference compounds, that is, Co_3O_4, CoO, and Co-foil. X-ray absorption near-edge spectra (XANES) were obtained by linear combination fitting of the Co_3O_4, CoO, and Co foil profiles. The coordination parameters for Co−Co and Co−O−Co shells were obtained by isolation of the respective shells from the EXAFS spectrum using the difference method outlined earlier by Miller et al.[52] The coordination numbers obtained through fitting the isolated shells are then divided by the fraction of that component obtained from XANES analysis for calculating the corrected coordination numbers.

2.2.5. Diffuse Reflectance Infrared Spectroscopy (DRIFTS). Operando diffuse reflectance Fourier transform infrared spectroscopy (DRIFTS) experiments were performed using a Thermo NICOLET 6700 FTIR spectrometer equipped with a liquid-nitrogen-cooled MCT detector and a KBr beam splitter. The DRIFTS cell consisted of a Smart Collector controlled-atmosphere chamber with ZnSe windows. Prior to the introduction of the steam reforming feed to the controlled-atmosphere chamber, there was a prereduction step, which consisted of heating the catalyst to 400 °C under a flow of He (30 ccm) for 30 min, followed by reduction for 2 h in 5% H_2/He (30 ccm) at the same temperature and purging with He (30 ccm) for 1 h at 450 °C. Following the aforementioned treatment step, the temperature was raised to 500 °C under helium flow, and the background spectra were collected every 50 °C, during cooling. At 25 °C, another background spectrum was collected and the ethanol steam reforming feed with a water-to-ethanol molar ratio of 10:1 and 0.3% ethanol concentration was introduced to the DRIFTS chamber. The feed stream was obtained by flowing helium through two separate bubblers containing water and ethanol kept at room temperature. At each temperature, the reaction was allowed to progress for 30 min before collecting sample spectra while reactants were still flowing through the DRIFTS chamber. After the collection of the sample spectrum, the DRIFTS chamber was flushed with helium for 8 min, and another sample spectrum was collected at the same temperature. Following the collection of this second spectrum, the temperature was increased under the reaction feed, and the procedure was repeated at 50 °C intervals up to 500 °C. Any oxygen impurity in helium was removed by an O_2 trap (VICI VALCO Instruments, HP2 He purifier) prior to feeding the gas to the DRIFTS chamber.

2.3. Catalytic Performance. *2.3.1. Steady State Catalytic Activity Testing.* The steady-state ethanol steam reforming activity data were collected in the 350−500 °C range using a fixed bed flow reactor system, which consisted of a feed system capable of delivering reactant mixtures of desired flow rates and compositions, a 4 mm-ID quartz reactor with a quartz frit, and an online gas chromatograph. For each run, a 9−50 mg batch of the Co/CeO_2 catalyst or the bare CeO_2 support was packed inside the reactor. The reactor was placed inside a resistively heated furnace (Carbolite, MTF 10/15/130), and the temperature was controlled by an Omega CSC232 PID temperature controller. Helium was used as the carrier gas, and the reactants were introduced to the helium stream using a heated evaporator-syringe pump assembly. The reactants, water and ethanol, at a 10-to-1 molar ratio, were fed to an evaporator maintained at 230 °C, using pulse-free syringe pumps (Cole-Parmer). The gas lines for the reactant gas stream were heated to 130 °C to prevent condensation. The steady-state reaction experiments were run in the kinetically controlled regime by maintaining the reaction conditions away from equilibrium at all temperatures. The Weisz−Prater criterion for internal diffusion effects and Mear's Criterion for external diffusion effects, were used to verify that there were no transport limitations in the system.

The reaction experiments were conducted with a feed stream concentration of 0.8% ethanol with 8% water in balance helium. The bed volumes in each experiment were fixed using silica as an inert diluent. The gas hour space velocity (GHSV) was kept constant at 72,000 h^{-1}. The catalyst comparisons were based on equal surface area in the reactor. Co/CeO_2 samples were run with 0.4 m^2, whereas the ceria supports were run with 0.8 m^2 surface area. All catalyst and support samples were subjected to the reduction pretreatments at 400 °C as described earlier in the section.

dx.doi.org/10.1021/cs3004159 | ACS Catal. 2012, 2, 2335−2348

For reactions with ethylene as the reactant, all parameters were kept identical, except replacing 0.8% ethanol with 0.8% ethylene.

The reported reactant conversion and product yield values are representative of the catalytic activity after steady state was reached at each temperature.

Ethanol conversion, hydrogen yield and selectivity of carbon containing species are defined as follows:

$$\text{EtOH conversion}(\%) = \frac{\text{moles of EtOH converted}}{\text{moles of EtOH fed}} \times 100$$

$$\text{H}_2\text{ yield}(\%) = \frac{\text{moles of H}_2\text{ produced}}{6 \times (\text{moles of EtOH fed})} \times 100$$

$$\text{Yield of C-containing product } i(\%) = \frac{(\text{no. of C atoms}) \times (\text{moles of } i \text{ produced})}{2 \times (\text{moles of EtOH fed})} \times 100$$

Similar definitions were used for conversion and product yields in ethylene reforming reactions.

The quantitative analysis of the reactor effluents was performed by online gas chromatography (Shimadzu Scientific 2010) equipped with a Carboxen column coupled with a pulsed discharge helium ionization detector (PDHID) which was used to separate and detect H_2, CO, and CO_2 and a Q-Bond column with a flame ionization detector (FID) to separate and detect the hydrocarbon species. The detectors were calibrated using samples of known concentrations, and the responses of the detector were recorded. The procedure was repeated at different concentrations to obtain a calibration curve. Calibration was repeated periodically. The carbon balances were always better than 95%.

2.3.2. Post-Reaction Temperature-Programmed Oxidation. Following stability and steady state reaction experiments, catalysts underwent a temperature programmed oxidation experiment to examine any carbon deposition on the surface. In these experiments, 15 mg of post reaction catalyst is loaded into a 4 mm-ID quartz reactor with a quartz frit and is heated in a Carbolite, MTF 10/15/130 furnace under a 30 ccm 10% O_2/He flow using a linear temperature program of 10 °C/min up to 500 °C. The reactor effluent was monitored via an MKS-Cirrus II online mass spectrometer for the mass signals of m/z = 32 for oxygen, m/z = 44 for carbon dioxide, and m/z = 28 for carbon monoxide. The CO signal was corrected for contribution from the CO_2 fragmentation.

2.3.3. Methanol Oxidation Pulse Reaction Experiments. Methanol oxidation experiments were conducted using Autochem II 2920. The feed and product analysis were performed with a MKS-Cirrus II online mass spectrometer for the mass signals of m/z = 30 for formaldehyde, m/z = 31 for methanol, and m/z = 44 for CO_2. Equal surface area of 2.24 m^2 was used for catalyst loading. The samples were prereduced as described in the previous section. Following reduction pretreatment, pulses of 4% methanol, 10% oxygen with balance He were fed to the reactor with a 1 mL sample loop. Feed and product pulses were analyzed by mass spectrometry. The signal for HCHO was corrected for contribution from the fragmentation of methanol. The signals were numerically integrated to compare and relate the peak areas to relative product concentrations.

3. RESULTS AND DISCUSSION

3.1. Characterization. *3.1.1. Surface Area, Pore Volume, and Dispersion.* Surface areas and pore volumes of the supported catalysts and bare supports are shown in Table 1. The commercial support as well as the Co/CeO_2(MP) catalyst was found to have significantly lower pore volume than the nanoparticles prepared by the hydrothermal method.

Table 1. Surface Area and Pore Volume of Bare Supports and Co/CeO_2 Catalysts Measured Using N_2 Physisorption

	BET surface area (m^2/g)	pore volume (cm^3/g)
CeO_2-MP	10	0.04
CeO_2-NP	100	0.17
Co/CeO_2-MP	9	0.03
Co/CeO_2-NP	56	0.12

Dispersion of metallic cobalt over both samples (shown in Table 2) was studied with Jensen's[51] method using N_2O as a probe molecule for chemisorption onto the reduced surface. 3% N_2O was fed to the sample following a reduction pretreatment, outlined in the previous section, thereby creating a mildly oxidizing atmosphere which has minimal chance of further oxidizing CoO species to Co_3O_4. Cobalt dispersion was found to be significantly higher with the Co/CeO_2(NP) with 24% as opposed to 2% with Co/CeO_2(MP) sample, indicating formation of smaller Co clusters on the nanoparticles. Since this technique probes only the metallic sites, it is also possible that the higher degree of reduction observed over the Co/CeO_2(NP) gives a higher dispersion value. It is more likely, however, that the observed difference is the culmination of both effects, that is, smaller particles and easier reducibility, as discussed in the following sections.

Table 2. Co Dispersion of Co/CeO_2 Catalysts Determined Using N_2O Chemisorption

	Co dispersion (%)
Co/CeO_2-MP	2
Co/CeO_2-NP	24

3.1.2. Transmission Electron Spectroscopy (TEM). A histogram of the particle size distribution for ceria supports with nano- and microsized particles is shown in Figure 1. The average particle sizes for CeO_2(MP) and CeO_2(NP) are 95 and 6.5 nm, respectively.

The digital micrographs of the bare ceria supports and the supported catalysts for the nano- and microparticle samples are shown in Figures 2 and 3, respectively. Figure 2a shows large particles of the bare support, with various sizes, ranging from 20 nm to 0.2 μm. Figure 2b shows Co/CeO_2(MP) particles where cobalt oxide particles were located on bulk ceria with limited dispersion. The same figure shows a Co_3O_4 particle positioned on a larger ceria particle, which allows for lattice fringe identification with 0.14 nm d-spacing, associated with the (220) Co_3O_4 plane (ICDD 42−1467). Figure 3a,b show CeO_2(NP) and Co/CeO_2(NP) micrographs where the particle size range is smaller, between 5 and 8 nm. Both ceria and Co_3O_4 particles were identified with lattice fringe diffractions with d-spacings of 0.31 nm for the (111) ceria plane (ICDD 81-792) and 0.29 nm for the (220) Co_3O_4 plane (ICDD 42-1467).

3.1.3. In Situ X-ray Diffraction (XRD). In situ XRD technique was used to investigate the reduction and reoxidation

dx.doi.org/10.1021/cs3004159 | ACS Catal. 2012, 2, 2335−2348

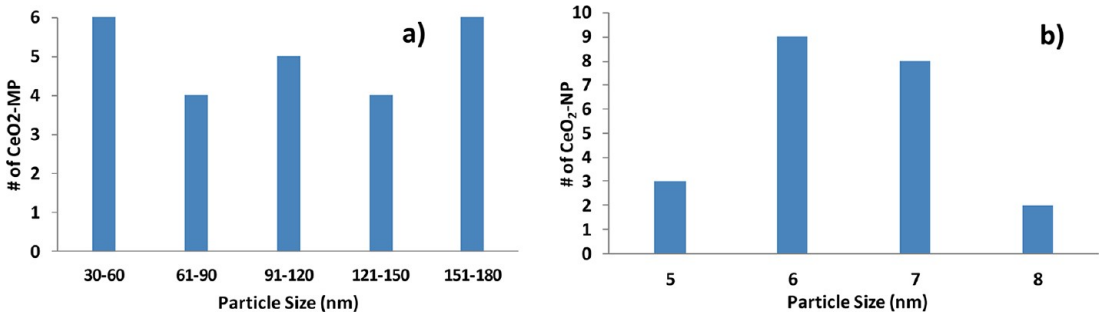

Figure 1. Particle size distribution histograms for (a) CeO_2(MP) and (b) CeO_2(NP).

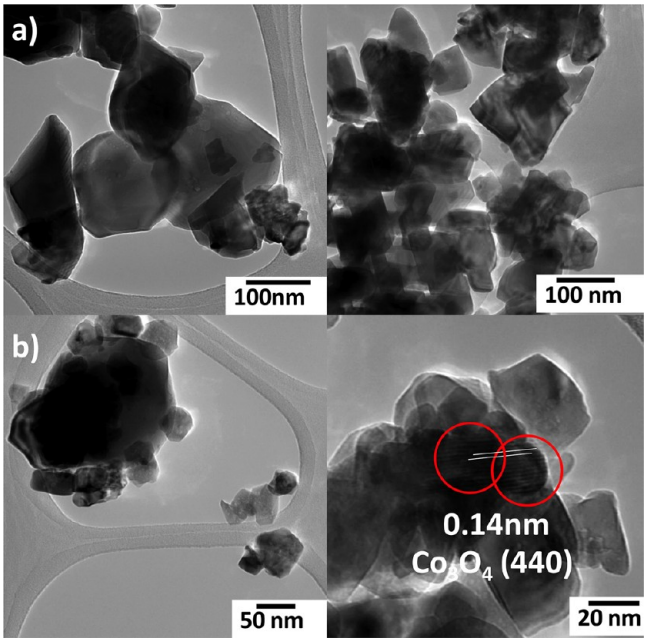

Figure 2. TEM images of (a) CeO_2(MP) bare support and (b) Co/CeO_2(MP) catalyst.

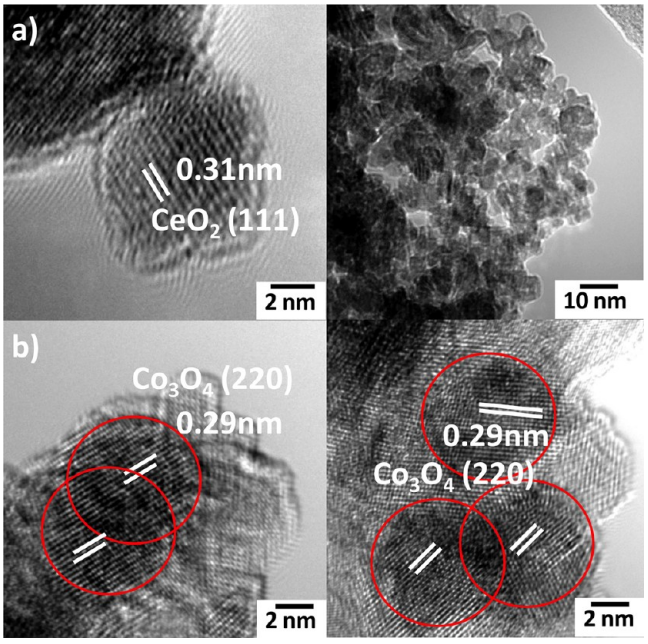

Figure 3. TEM images of (a) CeO_2(NP) bare support and (b) Co/CeO_2(NP) catalyst.

characteristics of Co/CeO_2(MP) and Co/CeO_2(NP) (Figures 4 and 5, respectively). Diffraction patterns were acquired during reduction at 50 °C intervals (Figure 4a and 5a). After the temperature was brought to room temperature and the reducing gas mixture was flushed from the in situ cell, an oxidizing gas mixture was introduced and diffraction patterns were taken during reoxidation at 50 °C intervals (Figure 4b and 5b). In all of the XRD patterns obtained, a well-resolved ceria peak was observed at 2Θ value of 33° which corresponds to the (200) plane in the face-centered cubic cerianite structure (ICDD #34-394). The ceria peaks persisted through reduction and oxidation and were the most prominent feature in the patterns.

Cobalt was observed in fully oxidized form prior to reduction as seen by the diffraction lines at 2Θ = 31° and 37°, which correspond to the (220) and (311) planes of Co_3O_4 planes, respectively (ICDD #42-1467). Additional diffraction lines corresponding to different Co species that emerged at different stages of reduction and oxidation processes and included a peak at 2Θ = 44° associated with the (111) plane of metallic cobalt (ICDD #15-806) and the weakly resolved peaks at 2Θ values of 36.5° and 42.4° signifying the (111) and (200) planes of CoO (ICDD #43-1004).

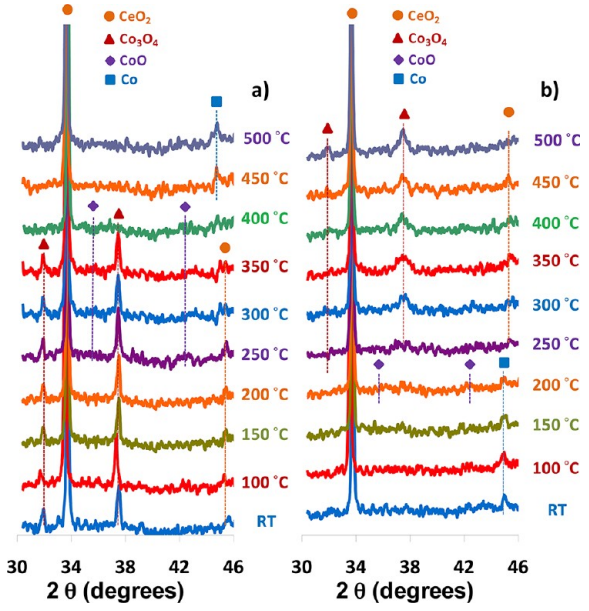

Figure 4. In situ X-ray diffraction patterns of Co/CeO_2(MP) taken during (a) reduction and (b) reoxidation.

dx.doi.org/10.1021/cs3004159 | ACS Catal. 2012, 2, 2335−2348

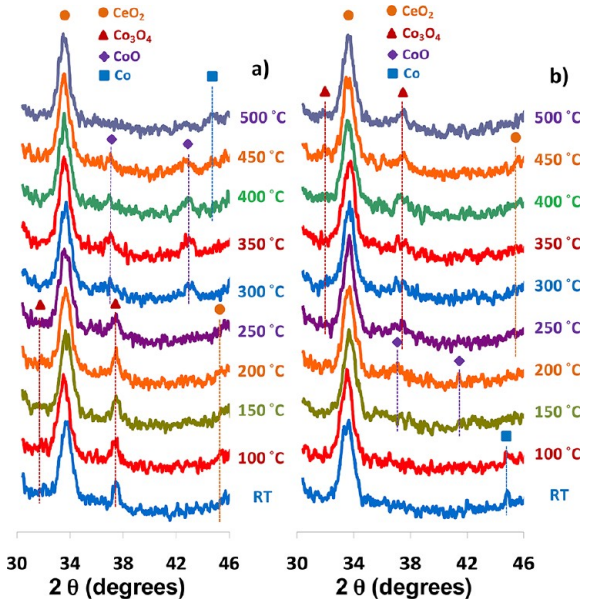

Figure 5. In situ X-ray diffraction patterns of $Co/CeO_2(NP)$ taken during (a) reduction and (b) reoxidation.

Although both catalysts exhibited these features at some stage of their reduction or oxidation process, there were significant differences between the diffraction patterns corresponding to the two samples. One of the pronounced differences was the significant line broadening exhibited by the $Co/CeO_2(NP)$ catalyst. Scherrer calculations have shown ceria particle sizes to be around 95 and 8.7 nm, for $Co/CeO_2(MP)$ and $Co/CeO_2(NP)$, respectively. The particle sizes for Co_3O_4 species were found to be around 25 and 5 nm for the same two samples. Peak broadening effect was fairly constant through the two temperature programs indicating negligible amount of catalyst or support sintering.

Although both catalysts in their pristine form were fully oxidized and showed Co_3O_4 and ceria peaks only, they were seen to reduce and reoxidize at different temperatures. During the reduction process of $Co/CeO_2(MP)$ (Figure 4a), diffraction lines corresponding to CoO were seen to emerge at 300 °C, and both Co_3O_4 and CoO phases were found to coexist up to 400 °C. Following the reduction at 400 °C, Co_3O_4 was no longer visible. Instead, a peak corresponding to metallic cobalt was observed at 44°. This behavior indicates a stepwise reduction of cobalt species from Co_3O_4 to CoO and finally into Co.[24] It is important to note that three oxidation states of Co were not seen to coexist at any temperature. The catalyst was fully reduced at 450 °C. After the pattern was collected at 500 °C, the sample temperature was decreased to room temperature and another diffraction pattern was collected (data not shown), and the sample was seen to retain its metallic character. Reoxidation of the sample in Figure 4b showed a rapid oxidation process, where the Co species were found to be metallic at 200 °C and fully oxidized at 250 °C, skipping of the CoO phase altogether. This suggests either a single step reoxidation of the cobalt species or a very rapid reoxidation where intermediate phases are short-lived.

Over the $Co/CeO_2(NP)$ sample, Co_3O_4 phase was observed to reduce at lower temperatures, indicated by the disappearance of the $2\Theta = 31°$ and 37° peaks above 250 °C. In comparison, these features were visible even at 350 °C with the $Co/CeO_2(MP)$ sample. Metallic cobalt formed between 350 and 400 °C and was seen to coexist with CoO phases up to 500 °C. The reoxidation profile in Figure 5b shows rapid reoxidation of the sample showing CoO species at temperatures as low as 150 °C. Co_3O_4 peaks form in the following temperature steps of 200 and 250 °C. The reduction of Co_3O_4, as well as reoxidation of the metallic cobalt into CoO was found to take place at lower temperatures for the $Co/CeO_2(NP)$ sample. The diffraction lines for Co species in this sample had a lower intensity compared to $Co/CeO_2(MP)$ sample, which may be due to the lack of long-range order in the small particles found in the $Co/CeO_2(NP)$ sample.

3.1.4. X-ray Absorption Spectroscopy (XAFS). The reducibility and the coordination environment of the Co catalysts were investigated via XAFS technique during in situ reduction of the samples at 400 °C under 3.6% H_2/He. Figure 6 presents

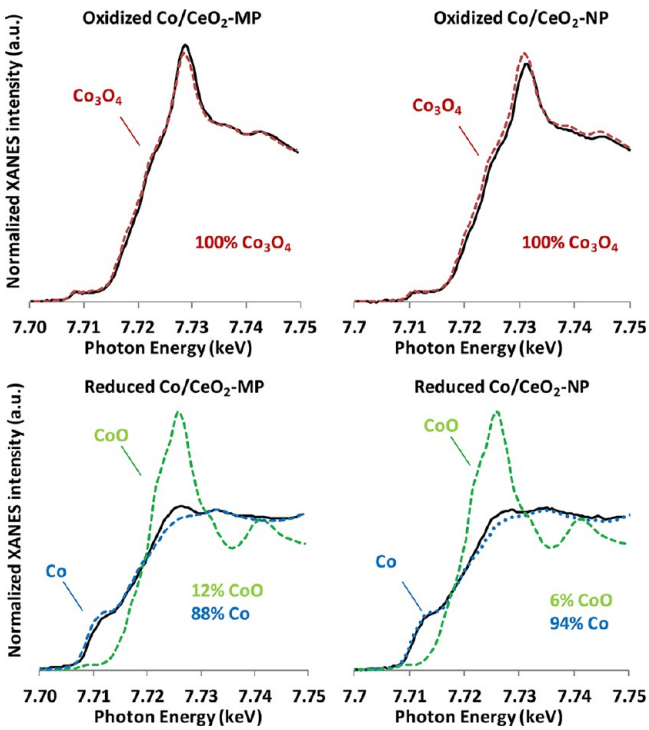

Figure 6. XANES spectra for oxidized and reduced $Co/CeO_2(MP)$ and $Co/CeO_2(NP)$.

the Co K-edge X-ray absorption near-edge spectra (XANES) collected over $Co/CeO_2(MP)$ and $Co/CeO_2(NP)$ catalysts before and after reduction pretreatment. Co_3O_4, CoO, and Co were used as reference compounds in linear combination fitting of the XANES region. The reference spectra are shown in Figure 6 together with the sample spectra to indicate the relative contribution of the cobalt states. Both samples have shown fully oxidized states of Co_3O_4 initially, and these spectra were fitted with Co_3O_4 reference only. The reduced samples were fitted with linear combinations of CoO and Co because of the two-step reduction scheme of cobalt species.[30,36,53−55]

Following 1 h of reduction, the $Co/CeO_2(NP)$ catalyst was found to be almost completely reduced to metallic Co within experimental error, whereas $Co/CeO_2(MP)$ sample consisted of 88% metallic Co and 12% CoO after the same pretreatment. The extent of reduction was found to be higher with the $Co/CeO_2(NP)$ sample which can be attributed to the small particle size and high metallic dispersion of the sample.

dx.doi.org/10.1021/cs3004159 | ACS Catal. 2012, 2, 2335−2348

Magnitudes of k^2-weighted Fourier transforms (FT) of the cobalt K-edge EXAFS spectra collected over Co/CeO_2(MP) and Co/CeO_2(NP) samples are shown in Figure 7. The 3.01 Å

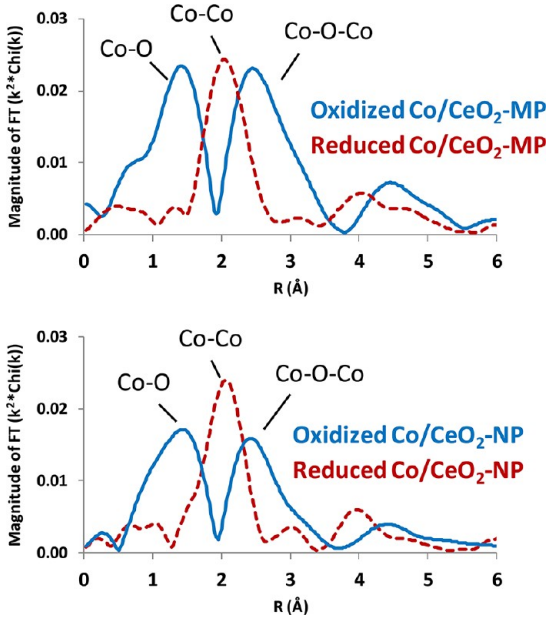

Figure 7. Magnitude of k^2-weighted Fourier transforms of cobalt K-edge EXAFS spectra.

region corresponded to Co−O−Co bridging atoms in an oxidized cobalt environment. This region is located at 2.5 Å on the figure because of the uncorrected nature of the Fourier transform. The Co−Co coordination around the 2.50 Å region (2.11 Å uncorrected) and the 2.11 Å (1.4 Å uncorrected) indicated metallic Co−Co shell and Co−O bond, respectively. Both samples have shown large peaks at the 2.11 and 3.01 regions prior to reduction, which is consistent with Co_3O_4 encountered in XANES. Following reduction, the Co−O region and Co−O−Co bridging region were still visible on the Co/CeO_2(MP) sample, indicating a more oxidized cobalt environmental state than Co/CeO_2(NP) which is consistent with the oxidation state information gained from the XANES region.

Table 3 summarizes the EXAFS fits on the FT magnitude spectra following the reduction pretreatment. The contributions of Co−Co were obtained by isolating the respective shell from the inverse FT. Co foil and CoO were used as the reference compounds and were analyzed by the same procedure. The coordination parameters obtained through fitting the EXAFS region for Co/CeO_2(MP) and Co/CeO_2(NP) were given in Table 3. The XANES data suggests that cobalt species exist in the form of Co and CoO; therefore, true coordination numbers were calculated by dividing the calculated fit by the fraction of the respective component from the XANES analysis. The fits suggest bulk-like particles for the Co species of the Co/CeO_2(MP) sample with a calculated coordination number (CN) of 11.0, whereas Co/CeO_2(NP) shows a Co−Co shell after reduction with a CN of 8.9, which indicates smaller metallic particle size for the sample. XAFS is a bulk technique, which can provide qualitative particle size comparison under in situ conditions. The CN information provides us with true in situ metallic particle size comparison for both samples.

Table 3. Results of EXAFS Fitting at the Co K-edge for the Co/CeO_2 Catalysts Following in Situ Reduction

sample	scatter	CN	CN fit	R (Å)	$\Delta\sigma$ (Å^2)	ΔE_0 (eV)
Co/CeO_2(MP)	Co−Co	11.0	9.7	2.50	0.008	−1.62
Co/CeO_2(NP)	Co−Co	8.9	8.4	2.49	0.007	−1.65

3.1.5. Operando DRIFTS during Ethanol Steam Reforming. The effect of ceria particle size on the evolution of surface intermediates and the reaction pathway during ESR over Co/CeO_2(MP) and (NP) catalysts was investigated in the temperature range of 25 °C−500 °C using DRIFTS. Operando DRIFT spectra collected while ethanol steam reforming reaction is progressing over the catalysts are presented in Figures 8a and 9a. Following each temperature step, the reaction chamber was flushed with He, and spectra were collected under He to identify the species remaining on the surface. These spectra are presented in Figures 8b and 9b.

Spectra collected over the two catalysts have many bands in common, although there are some noticeable differences as well. The 3600−3200 cm^{-1} broad band observed in all four figures is an indicator of surface hydroxyls and adsorbed water. It was visible upon introduction of the ethanol-steam feed mixture to the chamber at room temperature. Peak intensity is seen to diminish with temperature, and the peak disappears at 200 °C. The 1650 cm^{-1} band is associated with molecularly adsorbed water[3] and is not visible above 100 °C. A control experiment was conducted where pure steam was fed into the chamber (data not shown) and yielded the 1650 cm^{-1} peak as well as the rotational bands seen in the 1800−1300 cm^{-1} region. It should be noted that these localized bands seen in Figure 8a and 9a are independent of the signal-to-noise ratio and arise from the water vapor in the chamber, which is necessary for the true operando nature of the experiment. Upon flushing the chamber with He, these rotational bands disappear.

Figures 8a and 9a show several other bands which follow the same trends, namely, 2967 (2931 with NP), 1047 (1049), and 885 cm^{-1} bands were observed at 25 °C under the ethanol steam reforming reaction feed. These bands arise from interaction of ethanol with the catalyst surface and have been associated with ν_s (CH_3), ν (CO), and (C−C) stretch of surface ethoxy species, respectively. Formation of ethoxy species is indicative of dissociative adsorption of ethanol on the catalyst, yielding surface ethoxy and hydroxy species.[3,19,56−59] Most of the ethoxy species were not stable during helium flush.

Starting from 100 °C, both catalysts exhibit 1577 cm^{-1} and 1430 cm^{-1} bands which constitute the fingerprint region for ν_{as} (OCO) and ν_s (OCO) vibrations, respectively.[60] Although the water vapor makes it difficult to discern the peaks in Figures 8a and 9a, spectra taken after helium flush (Figures 8b and 9b) show the bands clearly. The presence of 1577 and 1430 cm^{-1} peaks throughout the temperature program suggests conversion of ethoxy species to surface acetate species which may further reform into carbonates.[36] It is difficult to distinguish carbonate species from acetates under actual reforming conditions. Disappearance of ethoxy species as well as the increase in intensity of the 2354 cm^{-1} and 2323 cm^{-1} CO_2 bands with increasing temperature suggests steam reforming is taking place on both samples. Spectra collected after He flushing show the surface carbonates to be stable up to 400 °C.

dx.doi.org/10.1021/cs3004159 | ACS Catal. 2012, 2, 2335−2348

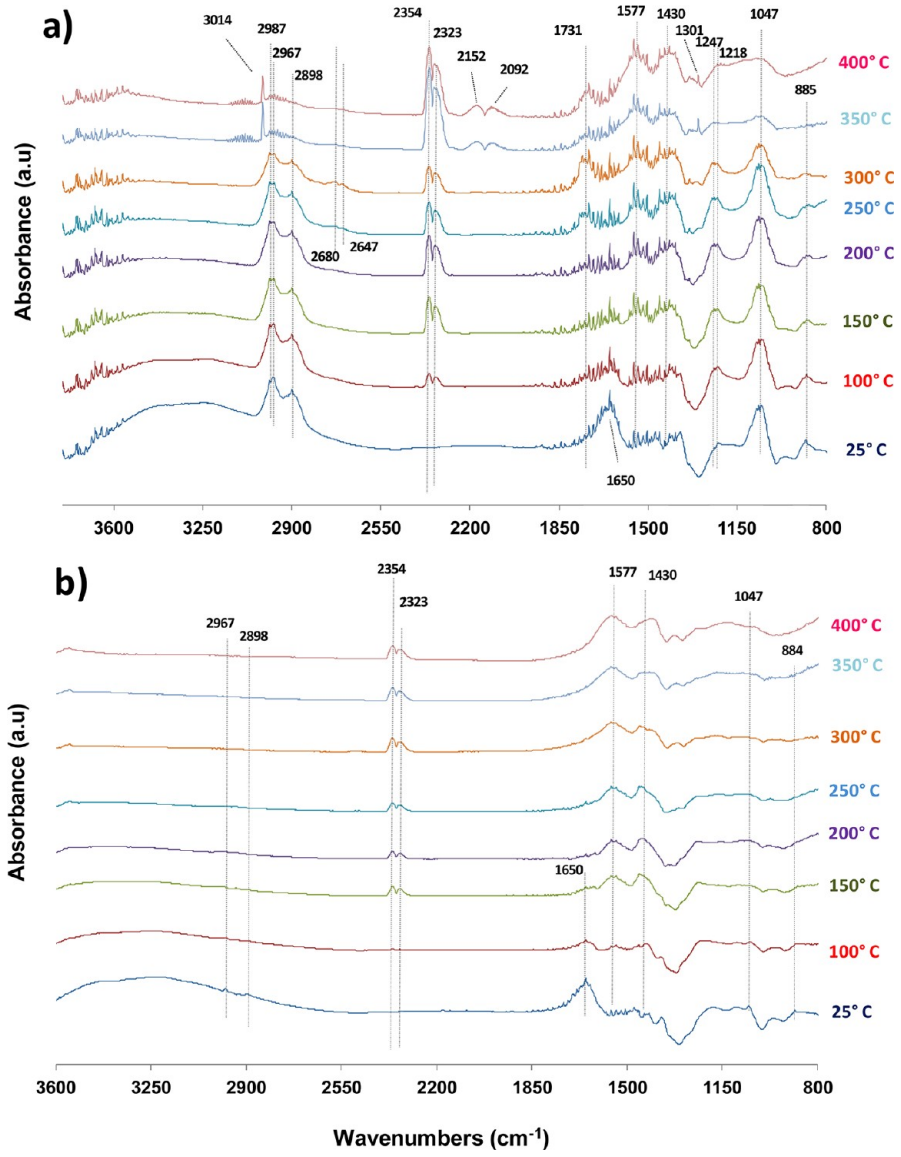

Figure 8. DRIFT spectra for $CoCeO_2$(MP) (a) during ESR and (b) after flushing with He.

Figure 8a of the Co/CeO_2(MP) sample shows a significant 3014 cm^{-1} band at 350 and 400 °C accompanied by bands at 1301 cm^{-1}, both of which are characteristic of methane. Concurrently with methane, 2152 and 2092 cm^{-1} bands appear, signaling CO formation. These may result from decomposition of ethanol into hydrogen, CO, and methane on the microparticle sample. Figure 9a shows much weaker bands at 3014 cm^{-1} and 1301 cm^{-1} even at 500 °C and has no CO bands.

Starting at 150 °C, 1336, 1012, and 933 cm^{-1} bands start to gain in intensity which indicate symmetric (CH_3) deformation and (CH_3) rocking. Along with the earlier discussion of the 1577 and 1430 cm^{-1} bands, these observations also support eventual reforming of surface species into acetates.[18,20,57]

Figure 8a shows formation of acetaldehyde species as identified by the 2680, 2647, and 1731 cm^{-1} bands, where the first two bands can be attributed to C−H stretching and the latter to the CO stretching of the aldehyde group. The acetaldehyde species indicate ethanol dehydrogenation reaction taking place on the sample starting from 250 °C. In the recent literature highly oxidized Co surfaces have been reported to favor ethanol dehydrogenation.[44,45] It should be noted that Co/CeO_2(NP) sample may also show dehydrogenation activity. However, the acetaldehyde species may not be stable at a more reduced surface. Figure 8b shows the acetaldehyde species to desorb easily after He flush at all temperatures. It should also be noted that the appearance of methane and CO peaks seen in Figure 8a coincides with the appearance of acetaldehyde species, suggesting that methane and CO may result from acetaldehyde decomposition as well.

Figure 8a shows additional bands at 2987 and 2898 cm^{-1}, which are in the CH_3 vibration region. An additional broad feature is around 1220 cm^{-1}. This band, which is not seen in Figure 9a, follows the same trend with the bands associated with ethoxy species and could be due to C−C bonds, and but it is difficult to identify it with certainty. Figure 9a shows, in addition to the 2964 cm^{-1} band, which is present over both samples, additional bands at 2856 and 2843 cm^{-1} in the CH_3 vibration region. The bands increase in their intensity first and then decrease with temperature and disappear at 200 °C. On the low wavenumber end of the spectra, a similar behavior is shown by the following bands: 1375 cm^{-1} $\delta_s(CH_3)$, and 1118,

dx.doi.org/10.1021/cs3004159 | ACS Catal. 2012, 2, 2335−2348

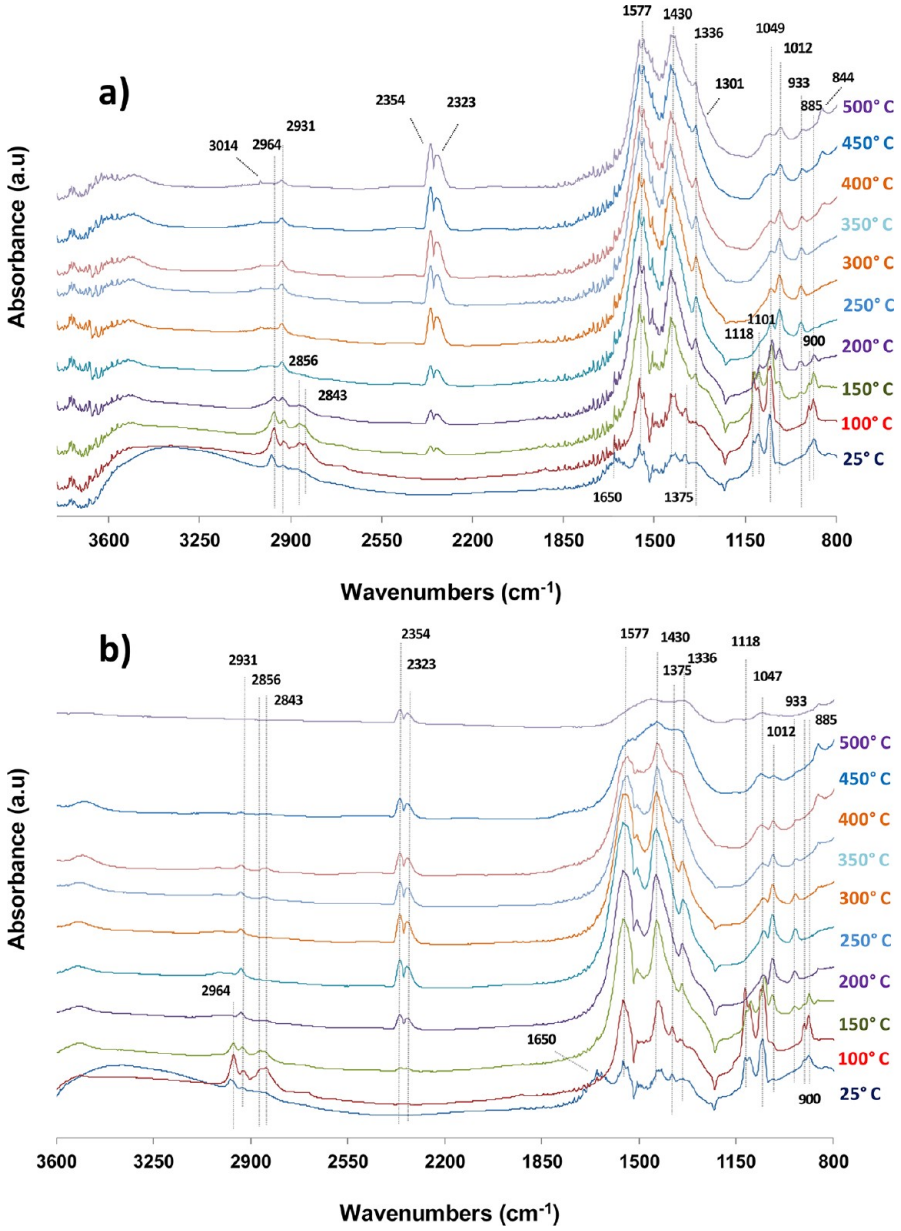

Figure 9. DRIFT spectra for $CoCeO_2$(NP) (a) during ESR and (b) after flushing with He.

1101, and 900 cm^{-1}. The last three bands do not show on the MP sample. The unambiguous assignment of the bands in this region is difficult. These bands may arise from CO vibrations, but they may also be attributed to the C−C stretching vibration of hydrocarbons. If it is the former, these bands would suggest different oxygenated species on the surface, which are not formed over the MP catalyst. However, the experimental results in the following sections suggest alkyl-type species. The 2856 and 2843 cm^{-1} bands, which show the same trends with the bands in the 900−1100 range, can be attributed to ethyl radicals,[61] which would indicate parallel formation of ethoxy and ethyl species at lower temperatures. As the temperature increases, ethoxy species persist through the temperature profile, which can be observed by the behavior of the 1049 and 2967 cm^{-1} bands. However, 2964, 2856, 2843, 1118, 1101, and 900 cm^{-1} bands disappear after 200−250 °C, suggesting a rapid conversion. Figure 9b shows the same species after He flush indicating strong surface vibrations. Kondo et al. have reported evolution of ethyl species following ethanol adsorption onto the catalyst surface[62] at 140 °C. Ethyl species may also be a precursor for ethylene,[63] as suggested by the same group. This may indicate an alternative pathway for ethylene production for the NP sample since these species are absent in Figure 8a,b. This observation is also consistent with the steady-state data, which will be discussed in the next section. Although ethyl species may offer an alternative route for ethylene formation, all other species observed in operando DRIFTS experiments are consistent with the reaction mechanism we have postulated earlier.[34]

3.2. Catalytic Performance: Steady State Catalytic Activity Testing. *3.2.1. Ethanol Steam Reforming Over Co/CeO_2 Catalysts.* Steady-state activity testing over Co/CeO_2(MP) and Co/CeO_2(NP) catalysts was performed to investigate the effect of cobalt and ceria particle size on ESR catalytic activity. Blank reactor experiments with the same feed conditions showed no detectable ethanol conversion within the

dx.doi.org/10.1021/cs3004159 | ACS Catal. 2012, 2, 2335−2348

Table 4. Steady State Catalytic Activity Data for ESR over Co/CeO_2(MP) and Co/CeO_2(NP) Catalysts[a]

	350 °C		400 °C		450 °C		500 °C	
products	MP	NP	MP	NP	MP	NP	MP	NP
% C_2H_5OH conversion	7.8	14.9	21.8	34.0	61.2	80.3	86.9	99.0
% H_2 yield	3.4	5.8	17.2	27.6	63.1	72.7	71.1	77.2
% yield								
CO_2	2.1	3.2	13.2	20.9	55.4	60.3	69.9	66.3
CO	0.4	0.6	2.1	1.0	4.0	1.5	13.2	7.2
CH_4	0.0	0.2	0.5	0.2	1.8	1.7	2.9	7.2
C_2H_4	0.2	0.3	1.5	2.8	0.0	13.7	0.0	18.6
C_2H_6	0.0	0.0	0.0	0.1	0.0	0.3	0.0	0.3
CH_3CHO	4.6	10.3	4.0	8.5	0.0	2.2	0.0	0.4

[a] C_{EtOH}= 0.8% and H_2O:EtOH = 10:1 (molar ratio) 0.4 m^2 total surface area. GHSV = 72000 h^{-1}.

tested temperature range of 350−500 °C (data not shown). Gas phase reforming was therefore assumed to be negligible within the experimental parameters.

The products formed over both catalysts included H_2, CO_2, CO, CH_4, C_2H_4, C_2H_6, and liquid products such as CH_3CHO and acetone where the latter is observed only in trace amounts. Reaction temperature and particle size was seen to significantly affect the product distribution. The reaction experiments were performed with equal surface areas as the basis, where the catalyst loadings were varied to achieve 0.4 m^2 surface area, which corresponded to 44.4 and 7.1 mg of Co/CeO_2(MP) and Co/CeO_2(NP) catalysts, respectively. The catalyst bed was diluted with an inert (silica) to maintain constant bed volume, and hence, constant gas hour space velocity (GHSV).

Table 4 presents the comparison of ethanol conversion levels, hydrogen yields, and selectivities for carbon containing products. The Co/CeO_2(MP) catalyst is observed to have relatively lower conversion and hydrogen yields compared to its nanoparticle counterpart at each temperature. However, the product distribution shows more striking differences between the catalysts. At 350 °C, both catalysts show acetaldehyde, which is the product of a dehydrogenation step, to be the main species in the product stream. As temperature increases, acetaldehyde yield decreases. At 400 °C, the Co/CeO_2(NP) sample has a higher reforming activity, and hence, a higher H_2 yield than the Co/CeO_2(MP). Both catalysts show increasing yields for CO and CH_4 with increasing temperature. These products may form from decomposition of aldehyde. However, the ratio is not one-to-one, suggesting other reaction steps for the production of carbon monoxide, including incomplete reforming. Both CO and CH_4 yields are higher over the Co/CeO_2(MP) compared to Co/CeO_2(NP).

An interesting feature of the product distribution is the high ethylene yield, which increases over both catalysts as the temperature is raised from 350 to 400 °C. At higher temperatures, ethylene is no longer observed over the Co/CeO_2(MP), whereas it continues to have the second highest yield among C-containing products over the Co/CeO_2(NP) catalyst. High ethylene yields suggest dehydration activity over both catalysts. Possible reaction steps that stem from ethylene include decomposition, which results in coking on the surface,[48,64−66] and ethylene reforming to H_2 and CO_x.[49,67−69] Both reactions have been reported on different catalytic systems.

When the catalysts were kept on stream at 500 °C, Co/CeO_2(MP) sample showed complete loss of activity within 12 h (Figure 10). The activity loss was accompanied by pressure build-up in the reactor, suggesting significant carbon deposition

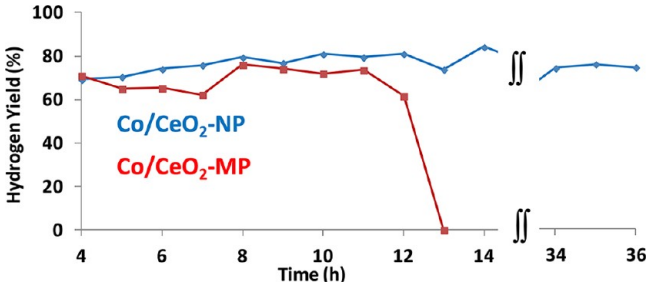

Figure 10. Time-on-stream performance of $CoCeO_2$(MP) and $CoCeO_2$(NP) during ESR.

over this catalyst. Co/CeO_2(NP) catalyst, on the other hand, showed no activity loss for 36 h, as seen in Figure 10. This result suggests that over the Co/CeO_2(NP) catalyst, the presence of ethylene does not lead to coke formation. It also suggests that Co/CeO_2(MP) catalysts have activity for both ethanol reforming and ethylene decomposition, which appear to proceed in parallel until the coke build-up becomes significant. This may be a phenomenon similar to the one reported in a recent review paper by Mattos et al.,[48] where cobalt-based catalysts exhibited high ESR activity despite formation of filamentous and amorphous carbon.

3.2.2. Post-reaction Characterization of Catalysts. To examine possible carbon deposition on the catalysts during ethanol steam reforming, post-reaction characterization experiments were performed. Catalysts that were kept on stream for 12 h were subjected to a temperature programmed oxidation process, where CO_x species evolving from the surface were monitored by mass spectrometry as a function of temperature. Figure 11 shows the m/z = 32, 44, and 28 signals that are traced for O_2, CO_2, and CO. CO profile has been corrected for the contribution from CO_2 fragmentation. The profiles are compared on the same scale. Co/CeO_2(MP) catalyst shows significantly higher CO_2 evolution over a wider temperature range compared to Co/CeO_2(NP), with two smaller peaks at 230 and 419 °C and a larger peak at 350 °C. The evolution of CO_2 at three different temperatures suggests different carbon species on the surface, with the low temperature peak corresponding to amorphous carbon and high temperature peaks corresponding to graphitic carbon.[70,71] Co/CeO_2(NP) catalyst shows much lower CO_2 evolution, with one major peak at 238 °C and a wide small peak at 419 °C, suggesting mostly amorphous carbon on this catalyst. When the profiles are deconvoluted using GRAMS AI spectroscopy software, more than 90% of carbon formed over the Co/CeO_2(MP) sample is seen to be graphitic whereas the carbon deposition on Co/

dx.doi.org/10.1021/cs3004159 | ACS Catal. 2012, 2, 2335−2348

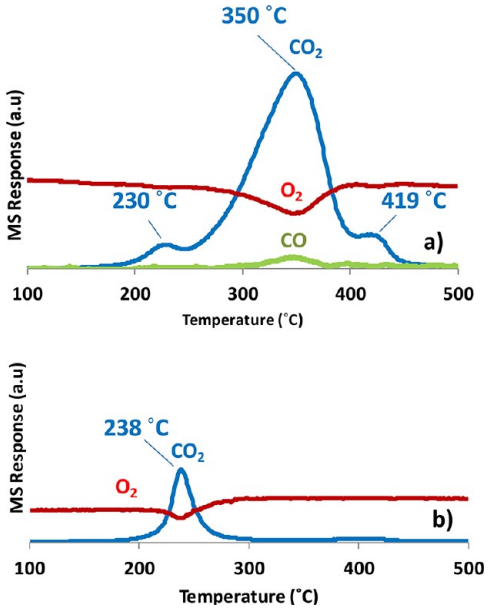

Figure 11. Temperature-programmed oxidation profiles after 12 h time on stream at 500 °C in ethanol steam reforming (a) Co/CeO_2(MP) and (b) Co/CeO_2(NP).

CeO_2(NP) catalyst was primarily amorphous. When the areas under the curve are compared, the Co/CeO_2(MP) sample shows more than 7 times more carbon deposition during the same length of time on stream.

Figure 12 shows post-reaction TEM images of the Co/CeO_2(MP) and Co/CeO_2(NP) samples. Carbon deposition is

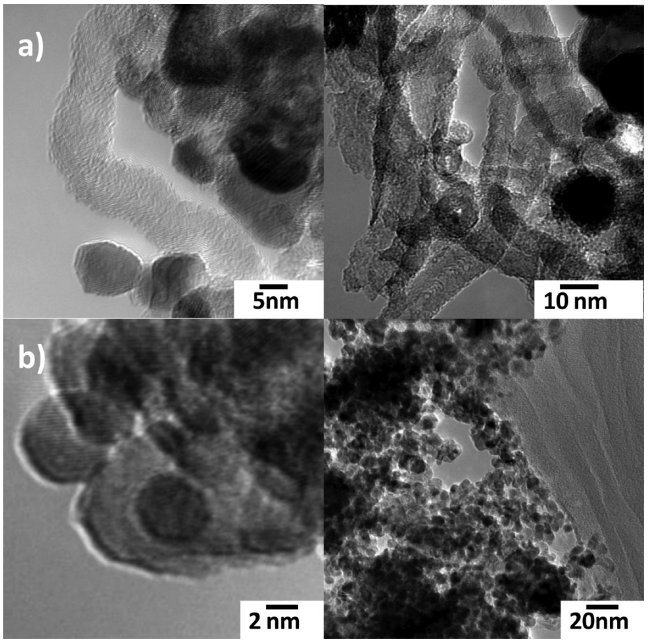

Figure 12. TEM images taken after ESR (a) Co/CeO_2(MP) and (b) Co/CeO_2(NP).

quite apparent on the Co/CeO_2(MP) sample mainly in the form of filament growth. Co/CeO_2(NP) micrographs show no sign of sintering of the ceria or cobalt particles. A typical metallic cobalt particle in Figure 12 shows a particle size of 4.5 nm. This is in agreement with the EXAFS fits in Table 3, which suggest small metallic particle size after reduction.

3.2.3. Ethanol Steam Reforming over CeO_2 Supports. Ethanol steam reforming activity of the bare CeO_2 supports were investigated with steady-state reaction experiments using the same parameters except the sample loading, which was increased to 0.8 m^2 to achieve conversion levels comparable to those attained over the supported catalysts used in this study. The reaction experiments were run using new reactors, which were not exposed to Co-containing species to eliminate the possibility of any cross contamination. Table 5 shows ethanol conversion, H_2 yield, and the yield of carbon-containing products obtained over the two supports. The same species as the ones seen over the catalysts were encountered in the product stream with significantly different product distributions. Both supports were found to have significant activity, especially at higher temperatures. However, the C−C bond cleavage activity was seen to be low. The major product over both supports was ethylene, but the yield of ethylene was much higher over CeO_2(NP), suggesting a high activity for ethanol dehydration. Methane was found to be another product which was abundant especially at higher temperatures. These experiments confirmed the active participation of the ceria support in ethanol steam reforming, as was reported for other support materials.[17] These experiments also showed the importance of support particle size, with nanosize particles having higher overall activity for dehydration, but being resistant to coking.

3.2.4. Ethylene Steam Reforming over Co/CeO_2 Catalysts. Encountering significant ethylene yields, especially over the bare supports, led us to investigate steam reforming of ethylene for Co/CeO_2(MP) and Co/CeO_2(NP) samples using the same parameters as ethanol reforming reactions. The conversion and yield data are presented in Table 6. Co/CeO_2(MP) has shown rapid increase in pressure drop as the reaction continued through the isothermal steps. At 450 °C and above, steady state data could not be obtained because of the pressure build-up in the reactor over this catalyst although no pressure build-up problem was encountered over the Co/CeO_2(NP) sample. The results indicate significant ethylene reforming activity over the Co/CeO_2(MP) sample, especially at lower temperatures, with CO_x and H_2 being the only products. At higher temperatures, however, ethylene decomposition becomes more prominent, which eventually leads to catalyst deactivation. Co/CeO_2(NP), on the other hand, was found to have very low ethylene reforming activity even at high temperatures; but there was not much cracking or decomposition activity, either. Coke formation over the Co/CeO_2-MP catalyst was verified by post-reaction temperature-programmed oxidation experiments (Figure 13), which showed significant carbon dioxide evolution at 180 and 350 °C. Post ethylene reaction TPO over the Co/CeO_2(NP) sample showed very little carbon deposition with a single CO_2 peak at 180 °C. These results help explain the product distribution over the two catalysts in ethanol steam reforming. It appears that although Co/CeO_2(NP) has dehydration activity, ethylene cracking does not proceed on this catalyst, rendering it highly resistant to coking.

It appears that, not only the NP support has significant activity itself for dehydration, the catalyst supported on this support can catalyze further reforming of ethylene while suppressing its decomposition. It also appears that the differences in product distribution may partially stem from

dx.doi.org/10.1021/cs3004159 | ACS Catal. 2012, 2, 2335−2348

Table 5. Steady State Catalytic Activity Data for ESR over Bare Ceria Supports[a]

	350 °C		400 °C		450 °C		500 °C	
products	MP	NP	MP	NP	MP	NP	MP	NP
% C_2H_5OH conversion	0.8	6.8	4.5	33.3	25.3	63.4	49.1	86.5
% H_2 yield	0.0	2.2	1.3	7.9	7.0	11.5	12.8	16.0
% yield								
CO_2	0.0	1.7	1.4	7.0	6.8	12.0	15.7	18.9
CO	0.0	0.1	0.0	0.7	0.0	1.0	0.8	3.8
CH_4	0.0	0.0	0.0	1.4	0.5	7.6	5.8	15.8
C_2H_4	0.1	2.3	1.9	18.8	15.3	35.5	24.0	42.9
C_2H_6	0.0	0.1	0.3	0.8	2.5	1.1	3.2	1.3
CH_3CHO	0.0	2.2	0.0	3.9	0.0	5.1	0.0	3.0

[a] C_{EtOH}= 0.8% and H_2O:EtOH = 10:1 (molar ratio) 0.8 m^2 total surface area. GHSV = 72000 h^{-1}.

Table 6. Steady State Catalytic Activity Data for Ethylene Steam Reforming over Co/CeO_2(MP) and Co/CeO_2(NP) Catalysts[a]

	350 °C		400 °C		450 °C		500 °C	
products	MP	NP	MP	NP	MP	NP	MP	NP
% C_2H_4 conversion	7.5	0.9	16.9	2.0	N/A	4.6	N/A	8.9
% H_2 yield	6.7	0.8	14.8	2.0	N/A	2.7	N/A	5.1
% yield								
CO_2	6.2	0.9	13.1	2.1		2.8		5.0
CO	1.8		3.2			0.6		2.1
CH_4						1.0		1.5
C_2H_6						0.2		0.2

[a] $C_{Ethylene}$= 0.8% and H_2O:EtOH = 10:1 (molar ratio). GHSV = 72000 h^{-1}.

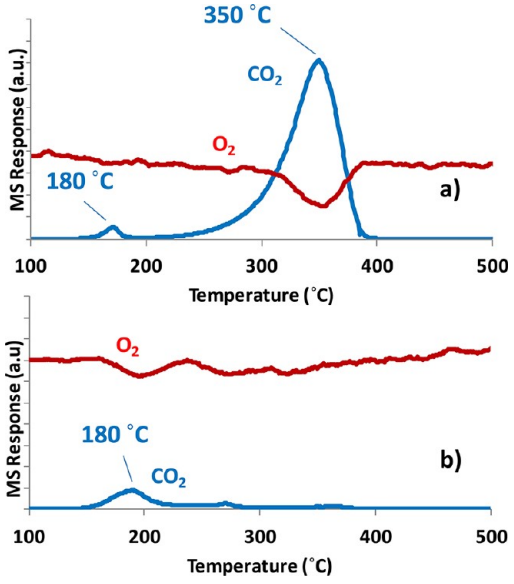

Figure 13. Temperature-programmed oxidation profiles after ethylene steam reforming reactions (a) Co/CeO_2(MP) and (b) Co/CeO_2(NP).

the differences in the support properties as well as the properties of the active phase itself.

In an effort to probe the surfaces of these two catalysts, pulse reaction experiments were performed using methanol oxidation as the probe reaction, as demonstrated for several catalytic systems by Wachs and co-workers.[72,73] CO_2 and HCHO were the only products resulting from the pulses. Table 7 shows the

Table 7. Methanol Pulse Oxidation

	relative selectivity for HCHO NP/MP
pulse 1	1.5
pulse 2	1.7
pulse 3	1.7
pulse 4	1.5

ratios of [relative HCHO selectivity for NP] to [relative HCHO selectivity for MP], which is defined as

$$\left\{\frac{\text{Area for HCHO}}{\text{Area for CO}_2}\right\}_{NP} / \left\{\frac{\text{Area for HCHO}}{\text{Area for CO}_2}\right\}_{MP}$$

"Relative HCHO selectivity" was calculated by dividing the area for HCHO by the area for CO_2. This ratio was, on the average, 1.6 times higher for the nanoparticle sample than for the microparticle sample. Since HCHO formation over oxides is associated with the redox sites, these results suggest a higher density of redox sites over the Co/CeO_2(NP) catalyst. Although these preliminary probing experiments provide some evidence of the relative abundance of different sites over the catalysts, the limited data do not allow any real quantification. Studies with probe reactions over the catalyst as well as the supports are in progress.

4. CONCLUSIONS

Co catalysts supported on two different ceria supports with particle sizes of 0.1−0.2 μm and 5−8 nm were examined for their ethanol steam reforming performance. In situ XRD and XAFS techniques showed higher reducibility with the Co/CeO_2(NP) catalyst. Steady-state activity tests showed significant differences in product distribution between the two samples, with the nanoparticle catalyst showing higher steam reforming performance despite high ethylene yields. Post-reaction studies as well as ethylene steam reforming activity tests showed the Co/CeO_2(MP) sample to have a high affinity for ethylene decomposition, and hence for coke formation where its counterpart was found to be highly resistant to coking. Operando DRIFTS studies suggested formation of different surface species on the samples, including some surface species which could be a precursor for ethylene. Pulse methanol oxidation experiments were performed to probe the surface sites of the catalysts. The results indicated a higher density of redox sites on the Co/CeO_2(NP) catalyst.

The nanoscale particle size of the support appears to lead to significant differences in the properties of the cobalt active phase. The smaller particle size also imparts the bare support

dx.doi.org/10.1021/cs3004159 | ACS Catal. 2012, 2, 2335−2348

with significant activity for ethanol dehydration. The superior performance of the cobalt catalysts supported on nanoparticles is thought to be due to a combination of factors, including increased reducibility, improved metal dispersion, and a difference in relative abundance of redox sites on the catalyst surface. All of these properties and, indirectly, the catalytic performance appear to be affected by the particle size of the support. It also appears that some of the differences observed in product distribution may have direct contributions from the activity of the nanoparticle support itself.

■ ASSOCIATED CONTENT

Supporting Information

The Co−Co shell fit for the reduced Co/CeO_2-MP and Co/CeO_2-MP samples are given in Figures SI-1 and SI-2. This material is available free of charge via the Internet at http://pubs.acs.org.

■ AUTHOR INFORMATION

Corresponding Author

*Phone: 614-292-6623. Fax: 614-292-3769. E-mail: ozkan.1@osu.edu.

Funding

We gratefully acknowledge the funding from the U.S. Department of Energy for the Grant DE-FG36-05GO15033. XAFS portion of this work was performed at the Dupont-Northwestern-Dow Collaborative Access Team (DND-CAT) located at Sector 5 of the Advanced Photon Source (APS). E.I. DuPont de Nemours & Co., The Dow Chemical Company, and the State of Illinois supported DND-CAT. Use of the APS was supported by the U.S. Department of Energy, Office of Science, Office of Basic Energy Sciences under Contract No. DE-ACO2-06CH11357.

Notes

The authors declare no competing financial interest.

■ ACKNOWLEDGMENTS

The authors also acknowledge Dr. Jeffrey T. Miller for his valuable insight, expertise, and help regarding XAFS portion of this study.

■ REFERENCES

(1) Haryanto, A.; Ferno, S.; Murali, N.; Adhikari, S. *Energy Fuels* **2005**, *19*, 2098−2106.
(2) Vaidya, P. D.; Rodrigues, A. E. *Chem. Eng. J. (Lausanne)* **2006**, *117*, 39−49.
(3) Mattos, L. V.; Noronha, F. B. *J. Catal.* **2005**, *233*, 453−463.
(4) Bshish, A.; Yaakob, Z.; Narayanan, B.; Ramakrishnan, R.; Ebshish, A. *Chem. Pap.* **2011**, *65*, 251−266.
(5) Ni, M.; Leung, D. Y. C.; Leung, M. K. H. *Int. J. Hydrogen Energy* **2007**, *32*, 3238−3247.
(6) F. Brown, L. *Int. J. Hydrogen Energy* **2001**, *26*, 381−397.
(7) de Lima, S. M.; da Cruz, I. O.; Jacobs, G.; Davis, B. H.; Mattos, L. V.; Noronha, F., B. *J. Catal.* **2008**, *257*, 356−368.
(8) Jacobs, G.; Keogh, R. A.; Davis, B. H. *J. Catal.* **2007**, *245*, 326−337.
(9) Scott, M.; Goeffroy, M.; Chiu, W.; Blackford, M. A.; Idriss, H. *Top. Catal.* **2008**, *51*, 13−21.
(10) Bonivardi, A.; Pistonesi, C.; Menghini, M.; Juan, A. *Comput. Mater. Sci.* **2000**, *18*, 39−47.
(11) de Lima, S. M.; Silva, A. M.; da Cruz, I. O.; Jacobs, G.; Davis, B. H.; Mattos, L. V.; Noronha, F. B. *Catal. Today* **2008**, *138*, 162−168.
(12) de Lima, S. M.; Silva, A. M.; Graham, U. M.; Jacobs, G.; Davis, B. H.; Mattos, L. V.; Noronha, F. B. *Appl. Catal., A* **2009**, *352*, 95−113.
(13) Dömök, M.; Baán, K.; Kecskés, T.; Erdőhelyi, A. *Catal. Lett.* **2008**, *126*, 49−57.
(14) Fierro, V.; Klouz, V.; Akdim, O.; Mirodatos, C. *Catal. Today* **2002**, *75*, 141−144.
(15) Fierro, V.; Akdim, O.; Provendier, H.; Mirodatos, C. *J. Power Sources* **2005**, *145*, 659−666.
(16) Salge, J. R.; Deluga, G. A.; Schmidt, L. D. *J. Catal.* **2005**, *235*, 69−78.
(17) Breen, J. P.; Burch, R.; Coleman, H. M. *Appl. Catal., B* **2002**, *39*, 65−74.
(18) Idriss, H. *Platinum Met. Rev.* **2004**, *48*, 105−115.
(19) Erdohelyi, A.; Rasko, J.; Kecskke, T.; Toth, M.; Domok, M.; Baan, K. *Catal. Today* **2006**, *116*, 367−376.
(20) Llorca, J.; Homs, N. *J. Catal.* **2004**, *227*, 556−560.
(21) Koh, A. C. W.; Leong, W. K.; Chen, L.; Ang, T. P.; Lin, J.; Johnson, B. F. G.; Khimyak, T. *Catal. Commun.* **2008**, *9*, 170−175.
(22) Llorca, J.; Homs, N.; Sales, J.; de la Piscina, P. R. *J. Catal.* **2002**, *209*, 306−317.
(23) Song, H.; Zhang, L.; Watson, R. B.; Braden, D.; Ozkan, U. S. *Catal. Today* **2007**, *129*, 346−354.
(24) Song, H.; Zhang, L.; Ozkan, U. S. *Green Chem.* **2007**, *9*, 686−694.
(25) Haga, F.; Nakajima, T.; Miya, H.; Mishima, S. *Catal. Lett.* **1997**, *48*, 223−227.
(26) Haga, F.; Nakajima, T.; Yamashita, K.; Mishima, S. *Nippon Kagaku Kaishi* **1997**, *11*, 758−762.
(27) Haga, F.; Nakajima, T.; Yamashita, K.; Mishima, S. *React. Kinet. Catal. Lett.* **1998**, *63*, 253−259.
(28) Pereira, E. B.; Homs, N.; Marti, S. *J. Catal.* **2008**, *257*, 206−214.
(29) Song, H.; Mirkelamoglu, B.; Ozkan, U. S. *Appl. Catal., A* **2010**, *382*, 58−64.
(30) Song, H.; Ozkan, U. S. *J. Mol. Catal. A: Chem.* **2010**, *318*, 21−29.
(31) Song, H.; Tan, B.; Ozkan, U. S. *Catal. Lett.* **2009**, *132*, 422−429.
(32) Song, H.; Ozkan, U. S. *J. Catal.* **2009**, *261*, 66−74.
(33) Song, H.; Ozkan, U. S. *J. Phys. Chem. A* **2010**, *114*, 3796−3801.
(34) Song, H.; Bao, X.; Hadad, C. M.; Ozkan, U. S. *Catal. Lett.* **2011**, *141*, 43−54.
(35) Song, H.; Zhang, L.; Ozkan, U. S. *Ind. Eng. Chem. Res.* **2010**, *49*, 8984−8989.
(36) Bayram, B.; Soykal, I. I.; von Deak, D.; Miller, J. T.; Ozkan, U. S. *J. Catal.* **2011**, *284*, 77−89.
(37) Zhou, X. D.; Huebner, W. *Appl. Phys. Lett.* **2001**, *79*, 3512−3514.
(38) Yi, N.; Si, R.; Saltsburg, H.; Flytzani-Stephanopoulos, M. *Appl. Catal., B* **2010**, *95*, 87−92.
(39) Si, R.; Flytzani-Stephanopoulos, M. *Angew. Chem., Int. Ed.* **2008**, *47*, 2884−2887.
(40) Yi, N.; Si, R.; Saltsburg, H.; Flytzani-Stephanopoulos, M. *Energy Environ. Sci.* **2010**, *3*, 831−837.
(41) Llorca, J.; Dalmon, J.-A.; Ramirez de la Piscina, P.; Homs, N. *Appl. Catal., A* **2003**, *243*, 261−269.
(42) Lin, S. S. Y.; Kim, D. H.; Engelhard, M. H.; Ha, S. Y. *J. Catal.* **2010**, *273*, 229−235.
(43) Martono, E.; Vohs, J. M. *J. Catal.* **2012**, *291*, 79−86.
(44) Hyman, M. P.; Vohs, J. M. *Surf. Sci.* **2011**, *605*, 383−389.
(45) Martono, E.; Vohs, J. M. *ACS Catal.* **2011**, *1*, 1414−1420.
(46) Yoon, S.; Kang, I.; Bae, J. *Int. J. Hydrogen Energy* **2008**, *33*, 4780−4788.
(47) Yoon, S.; Kang, I.; Bae, J. *Int. J. Hydrogen Energy* **2009**, *34*, 1844−1851.
(48) Mattos, L. V.; Jacobs, G.; Davis, B. H.; Noronha, F. B. *Chem. Rev.* **2012**, *112* (7), 4094−4123.
(49) Tanaka, Y.; Kato, T. *Appl. Catal., A* **2008**, *348*, 229−235.
(50) Zhou, K.; Wang, X.; Sun, X.; Peng, Q.; Li, Y. *J. Catal.* **2005**, *229*, 206−212.
(51) Jensen, J. R.; Johannessen, T.; Livbjerg, H. *Appl. Catal., A* **2004**, *266*, 117−122.

(52) Miller, J. T.; Marshall, C. L.; Kropf, A. J. *J. Catal.* **2001**, *202*, 89−99.
(53) Jacobs, G.; Ji, Y.; Davis, B. H.; Cronauer, D.; Kropf, A. J.; Marshall, C. L. *Appl. Catal., A* **2007**, *333*, 177−191.
(54) Llorca, J.; Piscina, P. R. d. l.; Dalmon, J.-A.; Homs, N. *Chem. Mater.* **2004**, *16*, 3573−3578.
(55) Pena O'Shea, d. l. V. A.; Homs, N.; Pereira, E.; Nafria, R.; Piscina, P. R. d. l. *Catal. Today* **2007**, *126*, 148−152.
(56) Llorca, J.; Homs, N.; Sales, J.; Fierro, J.; Luis, G.; Ramirez de la Piscina, P. *J. Catal.* **2004**, *222*, 470−480.
(57) Guil, J. M.; Homs, N.; Llorca, J.; de la Piscina, P. R. *J. Phys. Chem. B* **2005**, *109*, 10813−10819.
(58) Rasko, J.; Domok, M.; Baan, K.; Erdohelyi, A. *Appl. Catal., A* **2006**, *299*, 202−211.
(59) Idriss, H.; Scott, M.; Llorca, J.; Chan, S. C.; Chiu, W.; Sheng, P.-Y.; Yee, A.; Blackford, M. A.; Pas, S. J.; Hill, A. J.; Alamgir, F. M.; Rettew, R.; Petersburg, C.; Senanayake, S. D.; Barteau, M. A. *ChemSusChem* **2008**, *1*, 905−910.
(60) Yee, A.; Morrison, S. J.; Idriss, H. *J. Catal.* **1999**, *186*, 279−295.
(61) Haber, T.; Blair, A. C.; Nesbitt, D. J.; Schuder, M. D. *J. Chem. Phys.* **2006**, *124*, 054316−054316.
(62) Kondo, J. N.; Nishioka, D.; Yamazaki, H.; Kubota, J.; Domen, K.; Tatsumi, T. *J. Phys. Chem. C* **2010**, *114*, 20107−20113.
(63) Kondo, J. N.; Ito, K.; Yoda, E.; Wakabayashi, F.; Domen, K. *J. Phys. Chem. B* **2005**, *109*, 10969−10972.
(64) Rostrup-Nielsen, J. R. *Catal. Today* **1993**, *18*, 305−324.
(65) Rostrup-Nielsen, J. R.; Rostrup-Nielsen, T. *CATTECH* **2002**, *6*, 150−159.
(66) Takehira, K.; Ohi, T.; Shishido, T.; Kawabata, T.; Takaki, K. *Appl. Catal., A* **2005**, *283*, 137−145.
(67) Rangan, M.; Yung, M. M.; Medlin, J. W. *Catal. Lett.* **2012**, *142*, 718−727.
(68) Didenko, L. P.; Savchenko, V. I.; Arutyunov, V. S.; Sementsova, L. A. *Pet. Chem.* **2008**, *48*, 22−27.
(69) Graf, P. O.; Mojet, B. L.; van Ommen, J. G.; Lefferts, L. *Appl. Catal., A* **2007**, *332*, 310−317.
(70) Amorim, C.; Yuan, G.; Patterson, P. M.; Keane, M. A. *J. Catal.* **2005**, *234*, 268−281.
(71) Park, C.; Keane, M. A. *ChemPhysChem* **2001**, *2*, 733−741.
(72) Lee, E. L.; Wachs, I. E. *J. Catal.* **2008**, *258*, 103−110.
(73) Routray, K.; Zhou, W.; Kiely, C. J.; Wachs, I. E. *ACS Catal.* **2011**, *1*, 54−66.